11th International Symposium on Turbulence and Shear Flow Phenomena (TSFP11)
Southampton, UK, July 30 to August 2, 2019

THE EFFECTS OF THREE-DIMENSIONAL FORCING ON FLOW DEVELOPMENT WITHIN A LAMINAR SEPARATION BUBBLE

J. W. Kurelek[*] and **S. Yarusevych**[†]
Dept. of Mechanical and Mechatronics Engineering
University of Waterloo
Waterloo, ON, Canada, N2L 3G1
[*]jwukurelek@uwaterloo.ca
[†]syarus@uwaterloo.ca

M. Kotsonis
Faculty of Aerospace Engineering
Delft University of Technology
Delft, 2629HS, The Netherlands
m.kotsonis@tudelft.nl

ABSTRACT

This work examines flow development in a laminar separation bubble (LSB) undergoing natural transition and transition controlled with two-dimensional and spanwise modulated disturbances. The investigation is carried out in a series of wind tunnel tests, with the separation bubble formed over a flat plate subjected to an adverse pressure gradient. Velocity field measurements are performed using time-resolved, two-component Particle Image Velocimetry (PIV). Disturbances are produced using surface-mounted plasma actuators in a novel configuration that allows for the introduction of controlled disturbances that are two-dimensional or of a prescribed spanwise wavelength. The natural transition process is dominated by shear layer vortex shedding which is characterized by significant spanwise deformations in the aft portion of the bubble. When the flow is subjected to either two or three-dimensional forcing, vortex formation within the separation bubble is rendered two-dimensional. However, while the two-dimensionally forced perturbations remain largely two-dimensional until breakdown, a clear spanwise wavelength that matches the input wavelength of the forcing develops when the flow is subjected to the spanwise modulated forcing. The reported findings point to the presence of a secondary instability in the separation bubble, which leads to the amplification of the initially weak spanwise component of input disturbances, causing the shear layer vortices to develop significant spanwise undulations.

INTRODUCTION

Laminar separation bubbles are common in low Reynolds number flows, typically characterized by a chord-based Reynolds number of less than 5×10^5 (Carmichael, 1981). For these flows, the boundary layer is prone to separation when opposed by an adverse pressure gradient. If separation occurs, an unstable shear layer is formed and undergoes transition. Depending on flow conditions and geometry, the separated shear layer may reattach to the surface in a time-averaged sense, thus forming a closed region of recirculating fluid, referred to as an LSB. Due to a renewed interest in applications that commonly involve LSBs, such as small-to-medium scale turbo-machinery (Hodson & Howell, 2005) and unmanned aerial vehicles (Mueller & DeLaurier, 2003), recent research efforts have been focused on the laminar-to-turbulent transition process within the LSB so that, ultimately, the process may be controlled.

Numerous investigations have examined this transition process for LSBs formed over airfoils (*e.g.*, Burgmann & Schröder, 2008; Jones *et al.*, 2008; Boutilier & Yarusevych, 2012) and flat plates subjected to an adverse pressure gradient (*e.g.*, Watmuff, 1999; Alam & Sandham, 2000; Michelis *et al.*, 2018). In either configuration, the initial stage of transition is characterized by the amplification of small-amplitude disturbances in the separated shear layer, shown to be primarily due to an inviscid Kelvin-Helmholtz type instability (Watmuff, 1999; Boutilier & Yarusevych, 2012). Initially, disturbance growth is exponential and predominantly two-dimensional and thus good agreement has been found with linear stability theory (Alam & Sandham, 2000; Boutilier & Yarusevych, 2012). However, non-linear interactions begin to take place when disturbance amplitudes reach such substantially high levels, marking the later stages of transition.

A number of studies have shown the onset of the non-linear transition stage to coincide with the formation of coherent structures, as the separated shear layer rolls up into vortices that are shed at the frequency of the most amplified disturbances. This roll-up process has been observed experimentally (*e.g.*, Burgmann & Schröder, 2008; Hain *et al.*, 2009; Kurelek *et al.*, 2016) as well as numerically, (*e.g.*, Alam & Sandham, 2000; Jones *et al.*, 2008; Marxen *et al.*, 2013) with the formed structures dominating flow development in the aft portion of the bubble. At roll-up, the shear layer vortices have been found to be largely spanwise uniform, but then quickly undergo significant three-dimensional deformations prior to the breakdown to turbulence (Jones *et al.*, 2008; Marxen *et al.*, 2013; Kurelek *et al.*, 2016). In contrast, other investigators have reported highly deformed and spanwise non-uniform vortical structures at formation (Burgmann & Schröder, 2008; Hain *et al.*, 2009). Michelis *et al.* (2018) have recently proposed a theory that unifies these disparate descriptions, suggesting that the degree to which deformations occur in the vortex filaments depends on the relative amplitude between the normal and oblique modes that are active in the flow upstream of the LSB.

A more comprehensive understanding of LSB dynamics is desired since the most effective control strategies developed to-date have targeted the Kelvin-Helmholtz instability and the associated shear layer vortices. Many investigations have examined the effect of forcing on LSB dynam-

ics, with the prevailing technique being the introduction of periodic and spanwise uniform disturbances through wall oscillations (Alam & Sandham, 2000; Lang *et al.*, 2004), external acoustics (Jones & Sandberg, 2011; Kurelek *et al.*, 2018), or surface-mounted plasma actuators (Yarusevych & Kotsonis, 2017). Several investigators have linked the optimal excitation frequency to the frequency of the most amplified disturbances in the natural flow (*e.g.*, Marxen & Henningson, 2011; Yarusevych & Kotsonis, 2017), showing that inducing flow reattachment on a stalled airfoil (and thus forming an LSB) or reducing the size of an existing LSB is most effective when the excitation targets this frequency. When forcing at this 'fundamental' frequency, the vortex shedding process locks to the excitation frequency and the coherence of the structures is increased, which is related to a higher entrainment of momentum from the outer-flow to the surface, thus resulting in an upstream shift in the mean reattachment location.

Clearly, periodic disturbances aimed at controlled separation bubble dynamics can have a significant effect on the flow, however, the majority of the studies to-date have examined the problem in only two-dimensions while the flow development is inherently three-dimensional. Few investigators have pursued three-dimensional forcing of LSBs due to the difficulty in implementing the forcing technique in a reliable manner, which is then compounded by the need for three-dimensional flow field measurements. Such experiments were conducted, for example, by Lang *et al.* (2004), followed by a complimentary numerical simulation (Marxen *et al.*, 2003), with the prevailing conclusion being that three-dimensional forcing does not significantly affect LSB development, which is in contradiction with the recent findings of Michelis *et al.* (2018). Therefore, it is the aim of this investigation to experimentally examine the effects of controlled three-dimensional disturbances on an LSB. Deterministic three-dimensional forcing is achieved through the superposition of disturbances created by plasma actuators arranged in streamwise succession, and the flow field is assessed using time-resolved, two-component PIV.

EXPERIMENTAL SETUP

Experiments were conducted at Delft University of Technology in an open-loop, anechoic wind tunnel, the test section of which is 500×500 mm in cross-section and features a turbulence intensity of less than 0.04%. A schematic of the experiment is shown in Fig. 1. An acrylic flat plate, measuring $1000 \times 500 \times 20$ mm, was installed in the test section and an adjustable displacement body was used to condition the boundary layer on the top surface of the plate. The free-stream velocity was set to $U_0 = 5.5\,\mathrm{m\,s^{-1}}$, resulting in a Reynolds number of $Re_{\delta_s^*} = 730$ based on the displacement thickness at separation in unforced conditions, $\delta_s^* = 2.0$ mm.

Alternating current, dielectric barrier discharge (AC-DBD) plasma actuators were used to introduce controlled disturbances upstream of the LSB (Fig. 1). The actuators consisted of electrodes painted onto a polyethylene terephthalate (PET) dielectric layer using conductive silver paint. When operated, the actuators produce a weak wall-parallel jet at the interface where the high voltage and ground electrodes overlap (*e.g.*, Kotsonis *et al.*, 2011). The actuators had a total thickness of 410 µm and were recessed into the plate so as not to perturb the flow. Three-dimensional disturbances were produced by arranging two actuators in

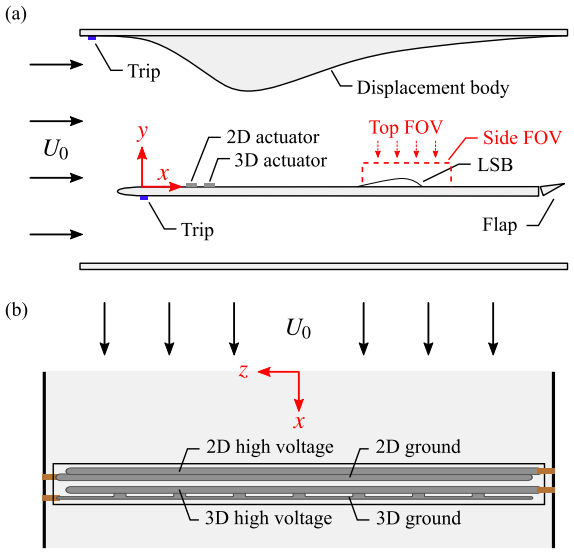

Figure 1. (a) Experimental setup and (b) detailed view of plasma actuator arrangement. Origin for indicated coordinate directions is located on the surface at the mid-span location where the flow separates in unforced conditions.

streamwise succession (Fig. 1b), with the upstream actuator used to produce a two-dimensional disturbance, while the downstream actuator forced in a spanwise modulated fashion as a result of the 50 mm gaps in its ground electrode. Note that the three-dimensional actuator was positioned such that the centre of an electrode overlap region was located at $z = 0$. Each actuator was driven by a dedicated TREK 20/20C high voltage amplifier fed by a National Instruments DAQ, thus allowing for adjustment of the phase delay between the two actuators. The forcing signals consisted of a 5 kHz sine wave amplified to 6 kV (peak-to-peak) and modulated by a 133 Hz square wave, with the modulation frequency matching the LSB fundamental frequency.

Time-resolved PIV measurements were performed in side (*x*-*y* plane) and top (*x*-*z* plane) view configurations (Fig. 1a). For the top-view configuration the laser sheet was positioned 7 mm from the top surface of the plate, while for the side-view, measurements were taken at multiple *x*-*y* planes so that the flow field could be volumetrically reconstructed using phase averaging. The flow was seeded with a glycol-water based fog with a mean particle diameter on the order of 1 µm and illuminated by a Continuum 532-120M Nd:YAG high-speed laser. Images were captured by a PCO Dimax HS4 camera fitted with a Nikon 105 mm macro lens set to a numerical aperture of 5.6. The fields of view were set to 80×16 mm and 135×67 mm for the side and top view configurations, respectively. The camera was synchronized with the laser via a LaVision timing unit, and image acquisition and processing was done using LaVision's DaVis 8 software. Double frame particle images were acquired using frame separation times that kept particle displacements under 15 px. Sampling was performed at 2 and 1.75 kHz for a total of 7238 and 4480 samples for the side and top view configurations, respectively. Prior to amplification, the plasma forcing signal was split and sent to the PIV timing unit, thus allowing for the phase information between the PIV acquisition and forcing to be determined.

For both PIV configurations, the imaged particles were approximately 3 to 4 px in diameter and an iterative, multi-

grid cross-correlation scheme with window deformation (Scarano & Riethmuller, 2000) was used to compute velocity fields. A final interrogation window size of 24×24 px with 75% overlap was used, with windows of this size containing, on average, 12 particles. As a result, the final vector pitches in the side and top view PIV data are 0.24 and 0.48 mm, respectively.

RESULTS

All presented results are non-dimensionalized using the displacement thickness at separation, $\delta_s^* = 2$ mm, and the free-stream velocity, $U_0 = 5.5\,\mathrm{m\,s^{-1}}$. All quantities non-dimensionalized by δ_s^* are accented with a tilde. Results are presented for three cases: (i) the natural (unforced) flow, (ii) two-dimensional forcing (spanwise wavelength, $\widetilde{\lambda}_z = 0$), and (iii) three-dimensional forcing with a spanwise wavelength of $\widetilde{\lambda}_z = 25$. Two-dimensional forcing was achieved through operation of only the upstream actuator using the previously specified forcing parameters. For the three-dimensional forcing, both actuators were operated simultaneously with a relative phase delay selected to produce superposition of the two disturbances introduced into the flow. The total momentum imparted to the fluid was kept constant between the two and three-dimensional forcing cases by using duty cycles of 25% and 23%, respectively.

Figure 2 presents contours of streamwise velocity measured using the top-view PIV configuration, where flow is from top-to-bottom. For these measurements, the laser sheet was positioned such that it passed through the top halves of the shear layer vortices, resulting in the capture of the structures as bands of relatively high streamwise velocity. For the natural case (Fig. 2a), strongly coherent spanwise vortices with significant spanwise undulations are apparent in the upstream portion of the FOV. Further downstream, structures of a similar spanwise wavelength are identifiable, however their spanwise coherence is decreased significantly. For the particular instant depicted in Fig. 2a, the predominant spanwise wavelength in the vortex filaments is approximately $\widetilde{\lambda}_z = 30$, which is roughly double the predominant streamwise wavelength, $\widetilde{\lambda}_x = 12.5$. It should be noted that significant variability is observed in the spanwise wavelengths of the naturally developing shear layer vortices, however the general range of observed wavelengths, $1 \lesssim \lambda_z/\lambda_x \lesssim 5$, is in agreement with previous LSB investigations (Marxen *et al.*, 2013; Kurelek *et al.*, 2018; Michelis *et al.*, 2018).

Significant changes in the flow development are observed when the flow is forced. Specifically, for the two-dimensional forcing (Fig. 2b) the most upstream vortex is uniform across the entire span. Further downstream, the vortex at $\widetilde{x} = 56$ is still largely two-dimensional, while having developed relatively small amplitude spanwise undulations and minor localized breakup regions, compared to the structure at the same streamwise location in the natural flow (Fig. 3a). Thus, the introduction of spanwise uniform disturbances targeting the primary LSB instability leads to increased spanwise coherence in the formed shear layer vortices, which persists as the vortices develop downstream. In a similar manner, the $\widetilde{\lambda}_z = 25$ case (Fig. 2c) shows a highly uniform vortex filament upstream of $\widetilde{x} = 50$. This indicates that the disturbances introduced into the flow are primarily two-dimensional with only a weak three-dimensional component, which is to be expected given that the disturbances

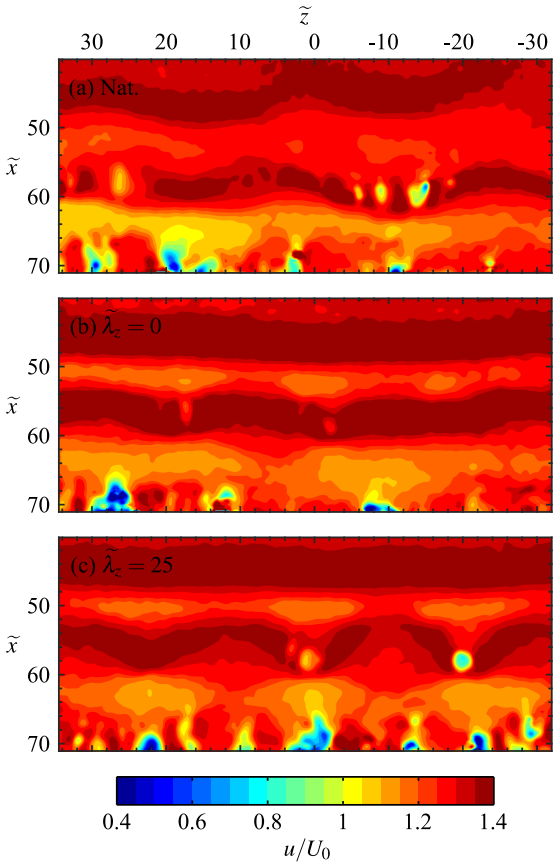

Figure 2. Instantaneous streamwise velocity contours. Flow is from top-to-bottom.

are introduced far upstream in the favourable pressure gradient region and oblique mode growth is expected to undergo less significant amplification compared to the normal mode (Michelis *et al.*, 2018). However, despite the relative weakness of the three-dimensional component, a spanwise wavelength that matches the forcing wavelength is evident in the downstream vortex. Note that the regions where the filament bulges forward are downstream of where the three-dimensional actuator is active, while the filament lags behind at spanwise locations downstream of the actuator gaps (Fig. 1b). The overall flow development depicted in Fig. 2c confirms a crucial aspect of this investigation, as the three-dimensional forcing does not result in a simple spanwise modulation of the base flow. Rather, the results point to the presence of a secondary instability in the LSB which amplifies the spanwise component of the input disturbances, causing the initially two-dimensional vortex filament to develop significant spanwise undulations at the prescribed wavelength.

Contours of phase-averaged spanwise vorticity, $\langle \omega_z \rangle$, measured using the side-view PIV configuration are presented in Fig. 3. Results for only the two and three-dimensional forcing cases are presented since phase-averaging is not possible for the natural case. To aid in visualizing the development of the shear layer vortices, the cores of vorticity upstream of $\widetilde{x} = 52$ are identified using the λ_2-criterion (Jeong & Hussain, 1995), which for a given structure are connected using a smoothing spline fit. The results in Fig. 3 affirm the observations made from the top-view PIV measurements (Fig. 2), as vortex filaments are initially two-dimensional under both types of forcing; how-

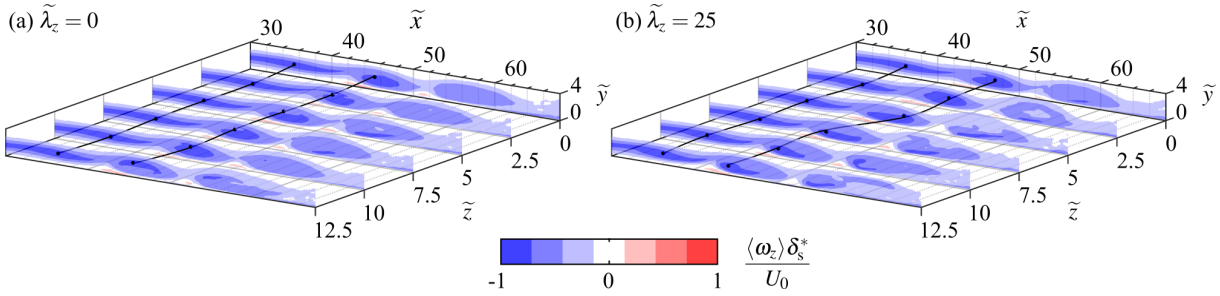

Figure 3. Phase-averaged spanwise vorticity contours for phase $\theta = 0°$ in the vortex shedding cycle. Dots mark vorticity cores for a given structure and are connected using smoothing spline fits.

ever, with downstream development a clear spanwise undulation develops for the $\widetilde{\lambda}_z = 25$ case (Fig. 3b) that is absent in the presence of purely two-dimensional forcing (Fig. 3a). Fig. 3b provides further insight into the effects of the three-dimensional forcing, as it shows the core of the shear layer vortex is closer to the surface in the region $\widetilde{z} \geq 7.5$, which is where the filament lags behind the streamwise forward bulge that develops within $\widetilde{z} \leq 5$. It is speculated that the small-amplitude three-dimensional modulations are amplified and lead to self-induced velocities causing lift-up and push-down in the regions where the filament bulges forward and lags behind, respectively. This, coupled with the strong shear near the wall, leads to a continual intensification of the vortex stretching, until localized vortex breakup takes place.

Previous investigators have demonstrated that the reattachment process in separation bubbles is almost entirely governed by the dynamics of the shear layer vortices (Marxen & Henningson, 2011; Yarusevych & Kotsonis, 2017), and so significant changes in the mean topology are expected as a result of the investigated forcing techniques. This is first examined through the contours of mean streamwise velocity, $\overline{u}$, from the side-view PIV measurements, presented in Fig. 4. The topology of the separation bubble is characterized using the dividing streamline, which forms a closed contour with the surface within which the streamwise mass flux is zero (Horton, 1968; O'Meara & Mueller, 1987). The intersection points of the dividing streamline with the surface give the mean separation, x_s, and reattachment points, x_r, with the former not being estimated as a result of lying well upstream of the measurement domain for all cases. The maximum bubble height, h, and its streamwise location, x_h, are also estimated, and are found where the maximum wall-normal distance between the surface and dividing streamline occurs.

The mean streamwise velocity contours in Fig. 4a shows the natural separation bubble reaches a maximum height of $\widetilde{h} = 0.8$ at $\widetilde{x}_h = 47.1$ and reattaches to the surface, in the mean sense, at $\widetilde{x}_r = 57.5$. Examining the same spanwise plane, $\widetilde{z} = 0$, when the flow is forced reveals small changes in the mean characteristics of the bubble for both the two and three-dimensional forcing cases, which is to be expected given the relatively small forcing amplitudes employed. That being said, both types of forcing do lead to slight upstream shifts in the maximum height and reattachment locations, which is consistent with previous reports on the effects of periodic forcing on separation bubble mean topology (Yarusevych & Kotsonis, 2017; Kurelek *et al.*, 2018). However, in these previous investigations forcing also leads to a reduction in the maximum bubble height, while the opposite is found here as the maximum

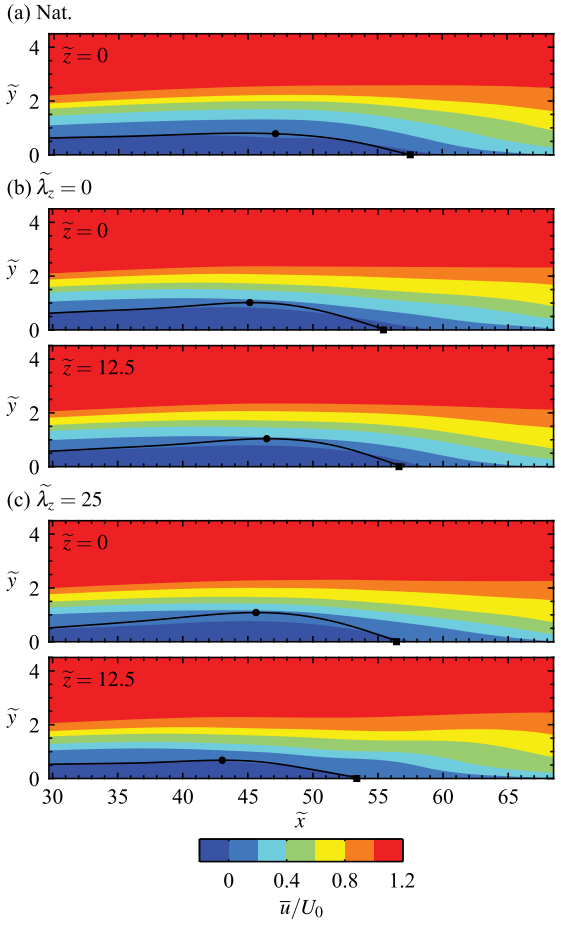

Figure 4. Mean streamwise velocity contours. Solid lines mark the dividing streamlines. Circle and square markers denote maximum bubble height and reattachment points, respectively.

bubble height increases to approximately $\widetilde{h} = 1.0$ for both the $\widetilde{\lambda}_z = 0$ and 25 cases.

With regards to the effect of the forcing on the spanwise topology of the bubble, Fig. 4b reveals negligible difference between the $\widetilde{z} = 0$ and 12.5 planes for $\widetilde{\lambda}_z = 0$ case, with the small differences between the maximum height and reattachment lying within the experimental uncertainty. Given this and the inevitable minor imperfections present in experiments, the mean bubble topology for this case can be considered essentially two-dimensional, which is to be expected given the type of forcing. In contrast, significant differences are observed between the $\widetilde{z} = 0$ and 12.5 planes

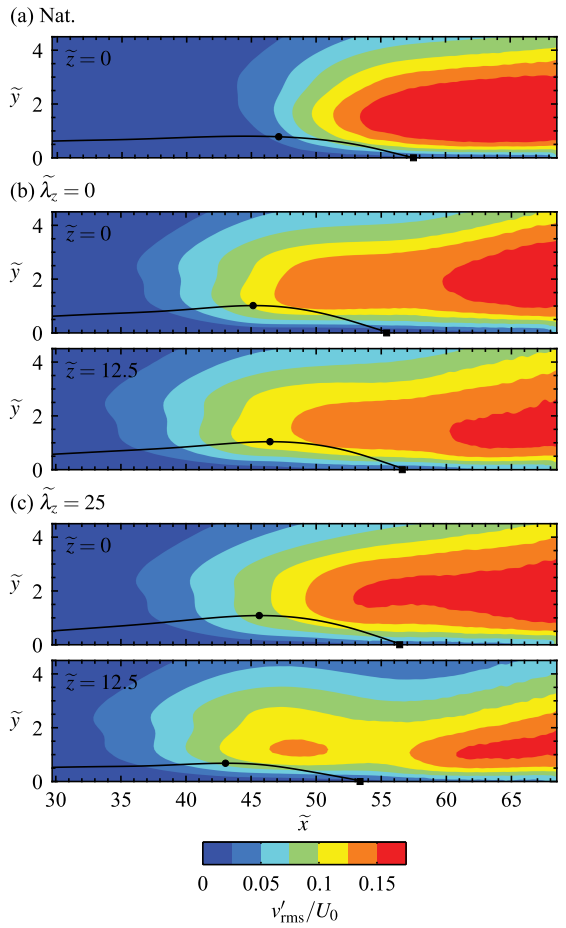

Figure 5. Rms of fluctuating wall-normal velocity contours. Solid lines mark the dividing streamlines. Circle and square markers denote maximum bubble height and reattachment points, respectively.

for the three-dimensional forcing case. The mean topology at $\widetilde{z}=0$ largely resembles that at the same plane for the two-dimensional case, while upstream shifts in x_h and x_r and a reduction in h is found at the $\widetilde{z}=12.5$ plane for the three-dimensional forcing case. These results indicate that the effects of three-dimensionality on the mean flow topology are most pronounced in regions where no superposition takes place between the produced disturbances, while in the regions where superposition does occur, the three-dimensional forcing acts in a similar manner to an equivalent, yet purely two-dimensional disturbance. Relating the changes observed in the mean topology of the bubble at $\widetilde{z}=12.5$ to the vortex dynamics, Fig. 3b shows that the shear layers vortices are pushed toward the surface in this region, which is consistent with the reduction in bubble height seen in Fig. 4c.

To further examine disturbance development within the bubble, contours of the root-mean-square (rms) of the wall-normal velocity fluctuations, v'_{rms}, are plotted in Fig. 5. Overall, the rms contours for the natural case (Fig. 5a) closely match previous reports for naturally developing separation bubbles (Yarusevych & Kotsonis, 2017; Kurelek *et al.*, 2018), with the streamwise amplification of disturbances first detected just upstream of the maximum height location, followed by strong growth in disturbance amplitudes in the aft portion of the bubble due to the shedding of the shear layer vortices. A similar trend is seen for the two-dimensional forcing case (Fig. 5b), albeit amplification is detected much further upstream as a result of the forcing targeting the primary instability within the bubble. Moreover, Fig. 5b provides further confirmation that the $\widetilde{\lambda}_z=0$ forcing is purely two-dimensional, as the rms contours for the $\widetilde{z}=0$ and 12.5 planes are largely the same.

Examining the v'_{rms} contours for the three-dimensional forcing case (Fig. 5c) reveals similar disturbance amplification for the $\widetilde{z}=0$ plane to that of the two-dimensional forcing case, although higher amplitude disturbances are found for the $\widetilde{\lambda}_z=25$ in the aft portion of the bubble, which may be related to an earlier onset of turbulent breakdown as a result of the intense vortex stretching that occurs (Fig. 3b). However, this does not impact the mean topology of the separation bubble, which is consistent with the arguments put forward by Kurelek *et al.* (2018), who contend that the location at which vortex formation occurs is the most significant factor influencing separation bubble topology, with the breakdown process only having minor influence. The strong effect of vortex formation and the associated dynamics on the rms contours is further reinforced at the $\widetilde{z}=12.5$ plane for the $\widetilde{\lambda}_z=25$ case. Here, as a result of the vortex being stretched and pushed toward the surface, a localized region of high v'_{rms} is found relatively close to the surface in the aft portion of the bubble. Further downstream at the mean reattachment point, the rms levels do not continuously rise, indicating that the forcing has interrupted the transition process in this region, which then resumes further downstream, as the rms levels begin to rise again at $\widetilde{x}=58$. It is noteworthy that disturbance growth in this region occurs in a region relatively close to the surface, compared to the natural and two-dimensional forcing cases, indicating the effects of the three-dimensional forcing are prevalent even far downstream of mean reattachment.

CONCLUSIONS

Flow development and the effect of controlled three-dimensional disturbances were investigated experimentally within a laminar separation bubble formed over a flat plate. The flow field was assessed in a series of wind tunnel tests carried out using time-resolved, two-component PIV. The measurements were performed in two separate configurations, allowing for the analysis of both streamwise and spanwise aspects of the flow development. The controlled disturbances were produced using surface mounted plasma actuators, with deterministic two and three-dimensional disturbances introduced via superposition of perturbations created by two actuators in streamwise succession. In total, three cases were investigated: (i) the natural (unforced) flow, (ii) two-dimensional forcing, and (iii) three-dimensional forcing with a spanwise wavelength of $\widetilde{\lambda}_z=25$. The total momentum imparted to the fluid was kept constant between the forcing cases.

Significant changes in the development of the shear layer vortices that form in the separation bubble were observed as a result of the forcing. When left to develop naturally, the vortices form with significant spanwise undulations, the wavelength of which exhibits a high degree of variability. When the flow is forced in a two-dimensional manner, vortex formation is essentially two-dimensional, with the vortex being uniform across the entire investigated span. This two-dimensionality is maintained as the vortex develops downstream, with only minor undulations developing prior to localized breakdown to turbulence. In a sim-

ilar manner, vortex filaments are initially spanwise uniform when the three-dimensional forcing is applied; however, substantial spanwise undulations develop downstream with a wavelength matching that induced by the forcing. These findings indicate that a secondary instability is present in the LSB, such that the weak three-dimensional component of the controlled perturbations is significantly amplified in the aft portion of the bubble, causing the initially two-dimensional vortex to develop significant spanwise undulations at the prescribed wavelength.

Further analysis of the vortex dynamics reveals that, in the case of the three-dimensional forcing, vortex filaments bulge forward in the region downstream of where superposition between the two actuators takes place, while the filaments lag behind and are pushed toward the surface downstream of where no superposition occurs. These filament motions, coupled with the strong shear near the wall, are speculated to lead a continual intensification of vortex stretching, leading to rapid filament deformation.

The discussed vortex dynamics are linked to the mean topological features of the separation bubble, as the two-dimensional forcing is shown to shift the mean maximum height and reattachment locations upstream, while also causing the mean bubble height to increase. Similar results are found for the three-dimensional forcing case at spanwise locations where the vortex filaments bulge forward, indicating that the effect of the forcing at these locations is similar to that from two-dimensional forcing. That being said, the most significant effects on the mean characteristics of the flow are seen in the regions the vortex filaments are pushed toward the surface, which in turn causes significant reductions in the maximum bubble height and disturbance growth to occur in a region much closer to the surface, even at locations downstream of mean reattachment.

ACKNOWLEDGEMENTS

The authors gratefully acknowledge the Natural Sciences and Engineering Research Council of Canada for funding this work.

REFERENCES

Alam, M. & Sandham, N. D. 2000 Direct numerical simulation of 'short' laminar separation bubbles with turbulent reattachment. *J. Fluid Mech.* **403**, 223–250.

Boutilier, M. S. H. & Yarusevych, S. 2012 Separated shear layer transition over an airfoil at a low Reynolds number. *Phys. Fluids* **24** (8), 084105.

Burgmann, S. & Schröder, W. 2008 Investigation of the vortex induced unsteadiness of a separation bubble via time-resolved and scanning PIV measurements. *Exp. Fluids* **45** (4), 675–691.

Carmichael, B. H. 1981 Low Reynolds Number Airfoil Survey. *Tech. Rep.*. NASA Contract Report No. 165803.

Hain, R., Kähler, C. J. & Radespiel, R. 2009 Dynamics of laminar separation bubbles at low-Reynolds-number aerofoils. *J. Fluid Mech.* **630**, 129–153.

Hodson, H. P. & Howell, R. J. 2005 The role of transition in high-lift low-pressure turbines for aeroengines. *Prog. Aerosp. Sci.* **41** (6), 419–454.

Horton, H. P. 1968 Laminar separation bubbles in two and three dimensional incompressible flow. PhD thesis, Queen Mary College, University of London.

Jeong, J. & Hussain, F. 1995 On the identification of a vortex. *J. Fluid Mech.* **285**, 69–94.

Jones, L. E., Sandberg, R.D. & Sandham, N. D. 2008 Direct numerical simulations of forced and unforced separation bubbles on an airfoil at incidence. *J. Fluid Mech.* **602**, 175–207.

Jones, Lloyd E. & Sandberg, Richard D. 2011 Numerical analysis of tonal airfoil self-noise and acoustic feedback-loops. *J. Sound Vib.* **330** (25), 6137–6152.

Kotsonis, M., Ghaemi, S., Veldhuis, L. & Scarano, F. 2011 Measurement of the body force field of plasma actuators. *J. Phys. D. Appl. Phys.* **44** (4), 045204.

Kurelek, J. W., Kotsonis, M. & Yarusevych, S. 2018 Transition in a separation bubble under tonal and broadband acoustic excitation. *J. Fluid Mech.* **853**, 1–36.

Kurelek, J. W., Lambert, A. R. & Yarusevych, S. 2016 Coherent Structures in the Transition Process of a Laminar Separation Bubble. *AIAA J.* **54** (8), 2295–2309.

Lang, M., Rist, U. & Wagner, S. 2004 Investigations on controlled transition development in a laminar separation bubble by means of LDA and PIV. *Exp. Fluids* **36** (1), 43–52.

Marxen, O. & Henningson, D. S. 2011 The effect of small-amplitude convective disturbances on the size and bursting of a laminar separation bubble. *J. Fluid Mech.* **671**, 1–33.

Marxen, O., Lang, M. & Rist, U. 2013 Vortex Formation and Vortex Breakup in a Laminar Separation Bubble. *J. Fluid Mech.* **728**, 58–90.

Marxen, O., Lang, M., Rist, U. & Wagner, S. 2003 A Combined Experimental/Numerical Study of Unsteady Phenomena in a Laminar Separation Bubble. *Flow, Turbul. Combust.* **71** (1-4), 133–146.

Michelis, T., Yarusevych, S. & Kotsonis, M. 2018 On the origin of spanwise vortex deformations in laminar separation bubbles. *J. Fluid Mech.* **841**, 81–108.

Mueller, T. J. & DeLaurier, J. D. 2003 Aerodynamics of Small Vehicles. *Annu. Rev. Fluid Mech.* **35** (1), 89–111.

O'Meara, M. & Mueller, Thomas J. 1987 Laminar separation bubble characteristics on an airfoil at low Reynolds numbers. *AIAA J.* **25** (8), 1033–1041.

Scarano, F. & Riethmuller, M. L. 2000 Advances in iterative multigrid PIV image processing. *Exp. Fluids* **29** (7), S051–S060.

Watmuff, J. H. 1999 Evolution of a wave packet into vortex loops in a laminar separation bubble. *J. Fluid Mech.* **31**, 119–169.

Yarusevych, S. & Kotsonis, M. 2017 Effect of Local DBD Plasma Actuation on Transition in a Laminar Separation Bubble. *Flow, Turbul. Combust.* **98** (1), 195–216.